Circulating mucosal associated invariant T cells identify patients responding to anti-PD1 therapy

Sara De Biasi
University of Modena
Lara Gibellini
University of Modena
Domenico Lo Tartaro
University of Modena and Reggio Emilia https://orcid.org/0000-0001-7762-2535
Emilia Mazza
Laboratory of Translational Immunology - Humanitas Clinical and Research Center
Simone Puccio
Humanitas Clinical Research Center
Jolanda Brummelman
Humanitas Clinical Research Center
Brandon Williams
Bio-Rad
Kelly Kaihara
Bio-Rad
Mattia Forcato
University of Padua
Silvio Bicciato
University of Modena and Reggio Emilia https://orcid.org/0000-0002-1944-7078
Marcello Pinti
University of Modena
Roberta Depenni
University of Modena
Roberto Sabbatini
University of Modena
Massimo Dominici
University of Modena and Reggio Emilia https://orcid.org/0000-0002-4007-1503
Giovanni Pellacani
University of Modena and Reggio Emilia https://orcid.org/0000-0002-7222-2951
Enrico Lugli
Humanitas Clinical and Research Center https://orcid.org/0000-0002-1964-7678
Andrea Cossarizza (andrea.cossarizza@unimore.it)

University of Modena https://orcid.org/0000-0002-5381-1558

Article

Keywords: Metastatic Melanoma, Biomarkers, Single-cell RNA-sequencing, Multiparameter Flow Cytometry, Tumor Microenvironment

Posted Date: October 8th, 2020

DOI: https://doi.org/10.21203/rs.3.rs-84729/v1

Version of Record: A version of this preprint was published at Nature Communications on March 15th, 2021. See the published version at https://doi.org/10.1038/s41467-021-21928-4.

Circulating mucosal associated invariant T cells identify patients responding to anti-PD1 therapy

Sara De Biasi[1*#], Lara Gibellini[1*], Domenico Lo Tartaro[1*], Emilia MC Mazza[2], Simone Puccio[2], Jolanda Brummelman[2], Brandon Williams[3], Kelly Kaihara[3], Mattia Forcato[4], Silvio Bicciato[4], Marcello Pinti[4], Roberta Depenni[5], Roberto Sabbatini[5], Massimo Dominici[1,5], Giovanni Pellacani[6], Enrico Lugli[2,7], Andrea Cossarizza[1,8#]

[1] Department of Medical and Surgical Sciences for Children & Adults, University of Modena and Reggio Emilia, Italy;
[2] Laboratory of Translational Immunology, Humanitas Clinical and Research Center - IRCCS, Rozzano, Milan, Italy;
[3] Bio-Rad Laboratories, 2000 Alfred Nobel Drive, Hercules CA, 94547;
[4] Department of Life Sciences, University of Modena and Reggio Emilia, Italy;
[5] Department of Oncology, University of Modena & Reggio Emilia, Modena, Italy;
[6] Department of Surgery, Medicine, Dentistry and Morphological Sciences, University of Modena and Reggio Emilia, Italy;
[7] Humanitas Flow Cytometry Core, Humanitas Clinical and Research Center - IRCCS, Rozzano, Milan, Italy;
[8] Istituto Nazionale per le Ricerche Cardiovascolari, via Irnerio 48, 40126 Bologna, Italy.

* equally contribution
# corresponding authors:
Prof. Andrea Cossarizza, MD, PhD
andrea.cossarizza@unimore.it
Phone: +39 059 2055401

Sara De Biasi, PhD
debiasisara@yahoo.it; sara.debiasi@unimore.it
Phone: +39 059 2055325

Abstract

Immune checkpoint inhibitors that maintain anti-tumor T cell response are used for treating patients with metastatic melanoma. Since the response to treatment is extremely variable, biomarkers are urgently needed to identify patients who could benefit from such therapy. We combined single-cell RNA-sequencing and multiparameter flow cytometry to determine changes in circulating $CD8^+$ T cells in patients with metastatic melanoma. A total of 28 patients starting anti-PD1 therapy were enrolled and followed for 6 months: 17 responded to therapy, whilst 11 did not. The proportion of activated and proliferating $CD8^+$ T cells and of mucosal associated invariant T (MAIT) cells was significantly higher in responders before starting therapy and was maintained over time. MAIT cells expressed higher level of CXCR4 and produced more granzyme B; *in silico* analysis revealed that they are present in the tumor microenvironment. Finally, patients with higher levels of MAIT showed a better response to treatment.

Introduction

CD8$^+$ T cells can drive adaptive immune responses against several types of human malignancies, in particular those with higher mutational burden and neoantigen load [1]. These cells are activated by tumoral antigens, undergo expansion, and can localize and kill infected or cancer cells. However, prolonged exposure to cognate antigens often contracts the effector capacity of T cells and attenuates their therapeutic potential. This process, collectively known as T cell exhaustion, is characterized by limited proliferation, cytokine production and effector capacity, metabolic rearrangement, increased inhibitory receptors expression and genome-wide accumulation of epigenetic modifications at effector and memory-related gene loci [2]. Among inhibitory receptors, programmed death 1 (PD-1) has been extensively studied, and is now targeted by therapies with monoclonal antibodies that are capable to reinvigorate T cells in several cancer settings. However, immune checkpoint inhibitors (ICI) mediate tumor regression only in a subset of patients, and the mechanisms at the basis of therapeutic resistance are poorly known [3]. A number of studies have initially focused on the mutational load of the tumor as well as on quality of the cells infiltrating the tumor microenvironment, and revealed that increased mutational burden and the presence of CD8$^+$ T cells with stem-like qualities [4, 5], among others, can predict the response to ICI [6-10]. However, tumoral tissue may not be always accessible, thereby making the quest of circulating biomarkers an absolute need. In this regard, recent studies have shown that responding patients have more large clones (those occupying >0.5% of repertoire) post-treatment than non-responding patients or controls, and this correlates with effector memory T cell percentage [11] suggesting that peripheral T cell expansion could predict tumour infiltration and clinical response [12].

Over the last decade, a pressing need to deeply interrogate immune cells either in the tumour microenvironment and/or in blood has led investigators to integrate data obtained from traditional approaches with those obtained with new, more advanced, single-cell technologies, capable to define characteristics of immune cells at an unprecedented degree of resolution [13]. Using single-cell RNA sequencing (scRNA-seq) and high-dimensional flow cytometry, we identify mucosal associated invariant T (MAIT) cells as possible biomarker of response to anti-PD-1 therapy in patients with metastatic melanoma.

Results

High-dimensional single-cell analysis of CD8+ T cells identifies higher percentage of activated effector memory T cells in responders

We initially used high-dimensional flow cytometry to longitudinally define the characteristics of T cells upon PD-1 blockade in melanoma patients **(Supplementary Figure 1)**. Computational analysis of aggregated data from multiple patients and time points identified twenty-eight clusters (individually labelled as C) among $CD8^+$ T cells, resolving a broad spectrum of T cell states, including maturation, activation and exhaustion. C21, C22, C26 display phenotypic identity proper of subsets of naïve T cells, characterized by expression of CD45RA, CCR7, CD27, CD28, negligible expression of CD25 and ICOS, and absence of additional markers [14] (**Figure 1A**). C28 represents recently activated T cells characterized by expression of CD38 and ICOS, but no expression of the late activation marker HLA-DR. T stem cell memory cells are identified in C10, and their phenotype is similar to that of naïve T cells, and includes the expression of CD95 [5,15]. C1, C20 and C27 represent $CCR7^+$,$CD45RA^-$ central memory T cells characterized by high expression of CD28, CD27, BTLA, CD194, CD25, CD95 and ICOS. C1 displays high levels of CD194, CD28, CD95 while C20 represents a cluster of T central memory (TCM) cells that expresses high level of CD39. C6, C17, C11, C2, C24, and C5 represent terminally differentiated T cells, being characterized by the expression of CD45RA, but not of CCR7, CD27, or CD28, and high levels of CD244, CD57 and T-bet. These cells also lacked granulysin expression.

C15, C4, C25, C14, C9, C13, C12, C19 and C16 represent effector memory T cell subsets characterized by the lack of expression of CD45RA, CCR7 and expression of CD25 and CD95 [16]. Among these, C14 expressed PD1 and CD57, and T-bet at intermediate levels, thereby suggesting the identification of replicative senescent cells [17]. C9, C13, C12 are transitional effector memory T cells as they express intermediate levels of CD28 and CD27 [18]. C9 expresses CXCR6, identifying effector memory cells with the capability to migrate to metastasis [19], while C12 is a cytotoxic T cell subset displaying high level of granulysin. C19 display high levels of CD127, CD39 and CD25, identifying not only metabolically activated, but also tumour-reactive cells [20]. C16 is a cluster of activated and proliferating effector memory T cells characterized by high level of expression of KI67, ICOS, CD95, HLA-DR, CD71, CD98, CXCR6, granulysin, CD38, intermediate expression of CD127, CD39, CD25, CD28, CD194, CD27, BTLA, T-bet and CD244; as shown in **Figure 1B**, this cluster was much more represented in responder patients if compared to non-responders.

Longitudinal analysis did not identify obvious differences in the dynamics of these immune populations between responders and non-responders to anti-PD-1 therapy (**Figure 1B**), except for

C16, identifying highly proliferating Ki-67+ CD71+ effector cells equipped for cytotoxicity ($GNLY^+$), whose relative frequency was higher in responder before starting therapy ($p<0.001$). This difference remained stable also after treatment ($p<0.01$) (**Figure 1B**).

MAIT cells are more abundant in responders as revealed by scRNA-seq

To further define the dynamics of T cells potentially involved in therapeutic response, we performed scRNA-seq of isolated $CD3^+$,$CD8^+$ T cells from a total of 20 patients at T0, T1 and T2 after anti-PD-1. After quality control, 55,200 cells were deemed suitable for analysis.
Contaminating 3,498 cells NK cells, expressing *TYROBP, FCGR3A, KLRB1* were removed from the analysis. We obtained a total of 51,702 purified $CD8^+$ T cells. Using a cTP-net, a deep neural network trained on multi-omics data, we imputed surface protein abundances within the scRNA-seq data to confirm T cell phenotype [21] **(Supplementary Figure 2)**.

Computational analysis identified eight different cell clusters on the basis of gene expression profiles (**Figure 2A and 2B;** see also **Supplementary file gene signature**). Naïve T cells were identified by expression of *LEF1, SELL, TCF7* genes while terminally differentiated effector memory cells, with cytotoxic properties were characterized by the expression of *GZMB, GNLY, NKG7, EFHD2* and *CXCR3* [22]. Two different clusters of effector memory cells were recognizable: one cluster of transitional effector memory (characterized by the expression of *GZMK* and *LYAR*) and one of more mature and activated phenotype with homing properties (expression of *TNFAIP3, CXCR4, CREM, CD69*) [23]. Two clusters of recently activated naïve T cells have been characterized: one expressed *GATA3* and *IL7R,* the other *FOS* and *JUN*. Activated and replicating effector memory T cell clusters were identified by the expression of *HLADRA, HLADRB1, CD74, GZMA, PCNA, MKI67, TOP2A, MCM4, MCM*. Finally, mucosal associated invariant T (MAIT) cells with homing properties were identified they expressed high level of *KLRB1, SLC4A10, MAF and CXCR4* [10,24].

Pseudotime analysis revealed that the differentiation process started from naïve T cells towards terminally differentiated T cells passing through activated naïve T cell, transitional effector memory T cells and effector memory T cells (**Supplementary Figure 3**). In this process, the transcriptionally distinct MAIT cells belong to a different branch of the Pseudotime trajectory compared to the rest of the T cells, albeit mapping close to effector memory T cells, in line with their shared phenotypic identity [25].

No main differences were found between R and NR in the amount of naïve, cytotoxic terminally differentiated and activated naïve T cells, both before and after therapy, as revealed by analysis of gene expression profiles by scRNA-seq (**Supplementary Figure 4**). The proportion of

activated effector memory T cells, reminiscent of C16 as defined by flow cytometry, was higher after two cycles of therapy in R compared to NR (**Figure 2C, left panel**). At the same time, activated effector memory T cells from R expressed higher levels of genes indicating activation (*FOS, DUSP1, FGFBP2, HLAC*) and cytotoxic behaviour (*GNLY*, *GZMH*), thereby suggesting heightened functional capacity in R (**Figure 2C, right panels**).

The proportion of MAIT cells was higher in R before therapy and after the first cycle of therapy (**Figure 2D, left panel**). This trend was visible also after the second cycle of therapy. Similarly to EM T cells, also MAIT cells showed overexpression of genes related to cell activation in R compared to NR before (*TNFAIP3, NKG7,NFKBIA, JUND, ZNF331, RGCC*) or after the first (*ZFP36L2, BTG1, ARL4C, CXCR4, ID2, FOS, ZFP36*) or the second cycle (*DUSP1, FOS, TNFAIP3, GZMK, JUND*) of anti-PD-1 therapy (**Figure 2D**, **right panels**), overall suggesting a dynamic regulation of MAIT cell activation over time.

Activated MAIT cells with homing properties are more abundant in responders.

We further subclustered MAIT cells before and after therapy to gain more insights into the cellular dynamics of these cells during the anti-tumor immune response. Our approach identified two different types of MAIT cells with differential expression of genes related to T cell activation or effector functions *DUSP1, ZFP36, TNFAIP3, ZFP36L2, FOS, CXCR4, NFKBIA, CD69*, *TSC22D3*, *BHLHE40* and *JUN*, thereby suggesting the identification of quiescent and activated subsets of cells (**Figure 3A, B**). In line with previous data, R showed a significantly higher proportion of activated MAIT compared to NR not only before therapy, but also after the first and the second cycle (**Figure 3C).**

We next used polychromatic flow cytometry to confirm these findings also at the protein level. In this regard, we analysed the percentage and phenotype of MAIT cells, identified as $CD3^{+}CD8^{+}$ T cells that expressed TCRα7.2 and CD161 (**Figure 4A**, **left**), and found marked expansion of these cells in the circulation of R patients when compared to NR before therapy (**Figure 4A**, **right**). This difference waned after therapy introduction in line with scRNA-seq data. Moreover, we found that the percentage of MAIT cells expressing the homing receptor CXCR4 increased after two cycles of therapy in R, but not in NR, that had a relevant variability (**Supplementary Figure 5**).

To confirm the presence of MAIT cells in the metastasis and primary tumour site we analyzed a public dataset available on Gene Expression Omnibus (GSE148190) [26]. This dataset contains single cell RNA and TCR sequencing of PBMCs and tumour-infiltrating lymphocytes from untreated patients with metastatic melanoma. We used the scRNAseq data of blood (B),

lymph nodes metastasis (LN) and Tumour (T) from patients K383, K409 and K411. A total of 26,757 cells have been analysed (11,614 of B, 12,915 of LN and 2,170 of T). About 3% of cells in LN and T were identified as MAIT cells expressing *CXCR4* gene, suggesting their ability to home the inflamed tissue **(Figure 4B, Supplementary Figure 6)**.

We next analysed the effector functional capacity of the MAIT cells following *in vitro* stimulation with IL-12, IL-18, CD3/CD28 followed by the detection of the effector molecules GRZM-B, IFN-γ and TNF **(Supplementary Figure 7)**. The overall quality of the response of MAIT cells, as assessed by combinatorial cytokine production, was largely similar between R and NR at different timepoints, where the majority of cells were capable to simultaneously produce GRZM-B, IFN-γ and TNF (**Figure 4C**). Nevertheless, before therapy, the percentage of cells able to produce only GRZM-B was higher in R if compared to NR (**Figure 4D**), thereby corroborating previous evidence that MAIT cells show preferential effector propensity.

Level of MAIT cells before therapy identifies responder patients.

We next evaluated the prognostic significance of the levels of MAIT cells in the circulation as predictive biomarker of the response to anti-PD-1 therapy. Flow cytometric analysis revealed that, within $CD8^+$ T cells, the median level of MAIT in the population of patients with metastatic melanoma was 1.7%, thus this value was used as a cut-off to stratify patients. **Figure 5** reports that patients with a frequency of MAIT cells >1.7% had an increased probability to respond than those patient with MAIT cells <1.7% (p=0.0363, Log-rank Mantel-Cox test).

Discussion

The main finding of our study is that patients who respond to ICI are characterized by a different composition of T cell subpopulations compared to those who do not respond, that are detectable before therapy initiation. The most relevant of these differences is at the level of MAIT cells, an innate population of $CD3^+$ T cells previously involved in early immunity against infection in peripheral tissue. Although the direct role of MAIT in mediating anti-tumor immune responses in melanoma is still under scrutiny, our data suggest that investigating MAIT cell frequency in the peripheral blood could be considered a possible predictive marker of successful therapy. Following introduction of ICI, R show differential dynamics of T cells compared to NR, involving the expansion of activated effector memory cells showing features of immune activation, proliferation and effector differentiation, as previously reported by other groups [27].

During the last decade, the immune response mediated by T cells in cancer patients assuming ICI has been deeply investigated by analysing both tumor-infiltrating lymphocytes and circulating T cells. Patients with melanoma or non-small cell lung cancer are characterized by an exhausted T cell phenotype along with impaired proliferation and low metabolic activation, and a high oligoclonal repertoire [28-30]. Activation of $CD8^+$ T cells has been considered a hallmark of response to therapy, and indeed after 1 cycle of therapy, Ki67 (a marker of cell proliferation) was found increased among effector memory cells [27, 31].

We show here that even if before treatment R and NR were characterized by similar clinical characteristic in terms of tumour burden and LDH level, activated effector memory T cells were more abundant in R, which can reflect a more activated CD8+ T cell compartment. This was particularly evident in MAIT cells. Circulating MAIT cells are a pro-inflammatory and cytotoxic population within effector memory T cells [32] and can represent up to 10% of peripheral $CD8^+$ T cells. They recognize microbial proteins presented by MR1 and display homing properties, as they express different homing and cytokine receptors. Furthermore, MAIT cells are deeply involved in patrolling mucosae and orchestrating the immune response in this environment [33].

The role of MAIT cells in cancer has been widely investigated. However, few studies have investigated their role during therapy with ICI. It was found that MAIT cells were decreased in blood and displayed an altered cytokine production in patients with cervical, colorectal, gastric, hepatocellular carcinoma, lung cancer and multiple myeloma. Moreover, controversial data exist on the prognostic benefit of MAIT cells in the tumour microenvironment, as it has been shown for instance in hepatocellular carcinoma [33]. Recent studies also show that MAIT cells promote tumour initiation, growth and metastases via tumour MR1 [34].

To the best of our knowledge, these are the first data that characterize MAIT cells in the peripheral blood of patients treated with anti-PD-1. We found that in R compared to NR, at baseline and after therapy introduction, i) the percentage of MAIT cells was higher; ii) MAIT cells displayed enhanced expression of genes related to immune activation and effector functions; iii) the percentage of MAIT cells expressing CXCR4 was higher in R after two cycles of therapy.

CXCR4-CXCL12 axis plays an important role in the interactions between cancer cells and their microenvironment. This axis modulates the traffic of tumor cells to metastasis, and mediates invasiveness, vasculogenesis and angiogenesis. However, pre-clinical melanoma models reported that this pathway can be influenced by anti-cancer treatments [35].

Hence, it is possible to hypothesize that, among other activities, the increased expression of CXCR4 on MAIT cells induced by anti-PD1 therapy could facilitate their migration towards metastases, where they could exert a pro-inflammatory and cytotoxic activity. To support this hypothesis, we observed that MAIT cells from R expressed CD69, which is not only an activation marker, but also a constitutively expressed marker of tissue residency. In immunotherapy-naive melanoma patients, the intratumor presence of $CD8^+$,$CD103^+$,$CD69^+$ T cells that are able to significantly increase during anti-PD-1 therapy has been associated with improved survival [36].

Very recently a population of MHC class-I-related molecule-restricted T cells belonging to the family of MAIT cells (defined "MR1" T cells) has been described as a rare population able to respond to a variety of tumor cells of different tissue origin, but not to microbial antigens [37]. Thanks to its ability to kill several cancer cell lines expressing low levels of MR1 while remaining inert to noncancerous cells, this population represents a subset with a great potential for cell therapy approaches in several malignancies [38, 39].

We are well aware that this study has some limitations. The first is represented by the relatively low number of patients enrolled in the study, the second by the lack of data regarding the characterization of MAIT in the tumour microenvironment, and the analysis of a possible mechanism responsible of a better prognosis. Thus, further studies are needed not only to confirm the utility of MAIT as biomarkers, but also to demonstrate their therapeutic potential or to provide actionable information about tumour's biology, which together holds great promise with respect to realising "personalized" treatment of melanoma.

In conclusion, we provide evidence of the association between the frequency and the effector functions of MAIT cells and the response to ICI in melanoma, thereby suggesting that the circulating levels of MAIT cells in the peripheral blood could serve as a useful, non-invasive biomarker. Future studies are needed to assess whether MAIT cells are directly involved in

mediating tumor regression that can be further amplified by targeting PD-1 or alternate immune checkpoints.

Acknowledgments

We thank Paola Paglia (ThermoFisher), Leonardo Beretta (Beckman Coulter), Federica De Paoli and Federico Colombo (Humanitas Clinical and Research Center, Rozzano, Milan, Italy) for the precious technical advices and continuous support. EL, SDB and LG have been or are Marylou Ingram Scholar of the International Society for Advancement of Cytometry (ISAC) for the period 2012-2016, 2016-2020, and 2020-2024 respectively. We are grateful to all the patients who donated blood for this study.

Authors' contribution

SDB, LG, DLT performed experiments and data analyses; EM, MF, SB, MP performed data analyses; RD, GP, RS enrolled the patients; BW, KK, JB, SP helped in setting up the methodology; SDB, LG, EL and AC designed the study; all authors discussed the data; SDB, LG, MD, EL and AC wrote the paper.

Funding

This work was supported by Fondazione Cassa di Risparmio di Modena to GP (2017); by Fondo di Ateneo per la Ricerca (FAR) 2017 to AC; by unrestricted grants to AC from: Sanfelice 1873 Banca Popolare (San Felice sul Panaro, Modena, Italy), Rotary CLUB Distretto 2072 (Modena, Modena L.A. Muratori, Carpi, Sassuolo, Castelvetro di Modena, Italy), Bio-Rad Laboratories (Hercules, CA, USA)

References

1. Topalian SL, Taube JM, Anders RA, Pardoll DM. Mechanism-driven biomarkers to guide immune checkpoint blockade in cancer therapy. *Nat Rev Cancer* **16**, 275-287 (2016).

2. Wherry EJ, Kurachi M. Molecular and cellular insights into T cell exhaustion. *Nat Rev Immunol* **15**, 486-499 (2015).

3. Havel JJ, Chowell D, Chan TA. The evolving landscape of biomarkers for checkpoint inhibitor immunotherapy. *Nat Rev Cancer* **19**, 133-150 (2019).

4. Brummelman J*, et al.* High-dimensional single cell analysis identifies stem-like cytotoxic CD8(+) T cells infiltrating human tumors. *J Exp Med* **215**, 2520-2535 (2018).

5. Lugli E, Galletti G, Boi SK, Youngblood BA. Stem, Effector, and Hybrid States of Memory CD8(+) T Cells. *Trends Immunol* **41**, 17-28 (2020).

6. Tumeh PC*, et al.* PD-1 blockade induces responses by inhibiting adaptive immune resistance. *Nature* **515**, 568-571 (2014).

7. Davoli T, Uno H, Wooten EC, Elledge SJ. Tumor aneuploidy correlates with markers of immune evasion and with reduced response to immunotherapy. *Science* **355**, (2017).

8. Miao D*, et al.* Genomic correlates of response to immune checkpoint therapies in clear cell renal cell carcinoma. *Science* **359**, 801-806 (2018).

9. Miao D*, et al.* Genomic correlates of response to immune checkpoint blockade in microsatellite-stable solid tumors. *Nat Genet* **50**, 1271-1281 (2018).

10. Sade-Feldman M*, et al.* Defining T Cell States Associated with Response to Checkpoint Immunotherapy in Melanoma. *Cell* **176**, 404 (2019).

11. Fairfax BP*, et al.* Peripheral CD8(+) T cell characteristics associated with durable responses to immune checkpoint blockade in patients with metastatic melanoma. *Nat Med* **26**, 193-199 (2020).

12. Wu TD*, et al.* Peripheral T cell expansion predicts tumour infiltration and clinical response. *Nature* **579**, 274-278 (2020).

13. Gibellini L, De Biasi, S., Porta, C., Lo Tartaro, D., Depenni, R., Pellacani, G., Sabbatini, R., Cossarizza, A. Singel-cell approaces to profile the response to immunecheckpoint inhibiotors. *Frontiers Immunology*, (2020).

14. Gattinoni L, Speiser DE, Lichterfeld M, Bonini C. T memory stem cells in health and disease. *Nat Med* **23**, 18-27 (2017).

15. Gattinoni L*, et al.* A human memory T cell subset with stem cell-like properties. *Nat Med* **17**, 1290-1297 (2011).

16. Mahnke YD, Brodie TM, Sallusto F, Roederer M, Lugli E. The who's who of T-cell differentiation: human memory T-cell subsets. *Eur J Immunol* **43**, 2797-2809 (2013).

17. Simonetta F*, et al.* High eomesodermin expression among CD57+ CD8+ T cells identifies a CD8+ T cell subset associated with viral control during chronic human immunodeficiency virus infection. *J Virol* **88**, 11861-11871 (2014).

18. Larbi A, Fulop T. From "truly naive" to "exhausted senescent" T cells: when markers predict functionality. *Cytometry A* **85**, 25-35 (2014).

19. Deng L, Chen N, Li Y, Zheng H, Lei Q. CXCR6/CXCL16 functions as a regulator in metastasis and progression of cancer. *Biochim Biophys Acta* **1806**, 42-49 (2010).

20. Duhen T*, et al.* Co-expression of CD39 and CD103 identifies tumor-reactive CD8 T cells in human solid tumors. *Nat Commun* **9**, 2724 (2018).

21. Zhou Z, Ye C, Wang J, Zhang NR. Surface protein imputation from single cell transcriptomes by deep neural networks. *Nat Commun* **11**, 651 (2020).

22. Kurtulus S*, et al.* Checkpoint Blockade Immunotherapy Induces Dynamic Changes in PD-1(-)CD8(+) Tumor-Infiltrating T Cells. *Immunity* **50**, 181-194 e186 (2019).

23. Zheng C, *et al.* Landscape of Infiltrating T Cells in Liver Cancer Revealed by Single-Cell Sequencing. *Cell* **169**, 1342-1356 e1316 (2017).

24. Guo X, *et al.* Global characterization of T cells in non-small-cell lung cancer by single-cell sequencing. *Nat Med* **24**, 978-985 (2018).

25. Leng T, *et al.* TCR and Inflammatory Signals Tune Human MAIT Cells to Exert Specific Tissue Repair and Effector Functions. *Cell Rep* **28**, 3077-3091 e3075 (2019).

26. Mahuron KM, *et al.* Layilin augments integrin activation to promote antitumor immunity. *J Exp Med* **217**, (2020).

27. Huang AC, *et al.* T-cell invigoration to tumour burden ratio associated with anti-PD-1 response. *Nature* **545**, 60-65 (2017).

28. Wieland A, *et al.* T cell receptor sequencing of activated CD8 T cells in the blood identifies tumor-infiltrating clones that expand after PD-1 therapy and radiation in a melanoma patient. *Cancer Immunol Immunother* **67**, 1767-1776 (2018).

29. Gide TN, *et al.* Distinct Immune Cell Populations Define Response to Anti-PD-1 Monotherapy and Anti-PD-1/Anti-CTLA-4 Combined Therapy. *Cancer Cell* **35**, 238-255 e236 (2019).

30. Schalper KA, *et al.* Neoadjuvant nivolumab modifies the tumor immune microenvironment in resectable glioblastoma. *Nat Med* **25**, 470-476 (2019).

31. Kamphorst AO, *et al.* Proliferation of PD-1+ CD8 T cells in peripheral blood after PD-1-targeted therapy in lung cancer patients. *Proc Natl Acad Sci U S A* **114**, 4993-4998 (2017).

32. Voillet V, *et al.* Human MAIT cells exit peripheral tissues and recirculate via lymph in steady state conditions. *JCI Insight* **3**, (2018).

33. Godfrey DI, Koay HF, McCluskey J, Gherardin NA. The biology and functional importance of MAIT cells. *Nat Immunol* **20**, 1110-1128 (2019).

34. Yan J, *et al.* MAIT Cells Promote Tumor Initiation, Growth, and Metastases via Tumor MR1. *Cancer Discov* **10**, 124-141 (2020).

35. Domanska UM, *et al.* A review on CXCR4/CXCL12 axis in oncology: no place to hide. *Eur J Cancer* **49**, 219-230 (2013).

36. Edwards J, *et al.* CD103(+) Tumor-Resident CD8(+) T Cells Are Associated with Improved Survival in Immunotherapy-Naive Melanoma Patients and Expand Significantly During Anti-PD-1 Treatment. *Clin Cancer Res* **24**, 3036-3045 (2018).

37. Lepore M, *et al.* Functionally diverse human T cells recognize non-microbial antigens presented by MR1. *Elife* **6**, (2017).

38. Crowther MD, *et al.* Genome-wide CRISPR-Cas9 screening reveals ubiquitous T cell cancer targeting via the monomorphic MHC class I-related protein MR1. *Nat Immunol* **21**, 178-185 (2020).

39. Mori L, De Libero G. 'Bohemian Rhapsody' of MR1T cells. *Nat Immunol* **21**, 108-110 (2020).

40. Cossarizza A*, et al.* Guidelines for the use of flow cytometry and cell sorting in immunological studies (second edition). *Eur J Immunol* **49**, 1457-1973 (2019).

41. Lugli E, Zanon V, Mavilio D, Roberto A. FACS Analysis of Memory T Lymphocytes. *Methods Mol Biol* **1514**, 31-47 (2017).

42. Chen H, Lau MC, Wong MT, Newell EW, Poidinger M, Chen J. Cytofkit: A Bioconductor Package for an Integrated Mass Cytometry Data Analysis Pipeline. *PLoS Comput Biol* **12**, e1005112 (2016).

43. Brummelman J*, et al.* Development, application and computational analysis of high-dimensional fluorescent antibody panels for single-cell flow cytometry. *Nat Protoc* **14**, 1946-1969 (2019).

44. Satija R, Farrell JA, Gennert D, Schier AF, Regev A. Spatial reconstruction of single-cell gene expression data. *Nat Biotechnol* **33**, 495-502 (2015).

45. Butler A, Hoffman P, Smibert P, Papalexi E, Satija R. Integrating single-cell transcriptomic data across different conditions, technologies, and species. *Nat Biotechnol* **36**, 411-420 (2018).

46. Zappia L, Phipson B, Oshlack A. Exploring the single-cell RNA-seq analysis landscape with the scRNA-tools database. *PLoS Comput Biol* **14**, e1006245 (2018).

47. Qiu X*, et al.* Reversed graph embedding resolves complex single-cell trajectories. *Nat Methods* **14**, 979-982 (2017).

48. Shen L, *et al*. GeneOverlap: Test and visualize gene overlaps. R package version 1.24.0. http://shenlab-sinai.github.io/shenlab-sinai/. (2020)

49. Roederer M, *et al.* SPICE: exploration and analysis of post-cytometric complex multivariate datasets. *Cytom. A* **79**, 167–174 (2011).

Methods

Patients

The study was conducted on 28 patients with metastatic melanoma treated with standard-of-care nivolumab or pembrolizumab. According to the RECIST, responders (n=17) were defined as patients with complete response (CR), partial response (PR), stable disease (SD), or mixed response (MR) of greater than 6 months with no progression, and non-responders (n=11) as patients with progressive disease (PD). In particular, among responders, 41.2% had CR, 35.3% had a PR, 17.6% had SD, and 5.9% (which corresponds to one patient) had a MR. The clinicopathologic characteristics of patients are reported in **Table 1**. The mean age of the total cohort was 71±12 years and plasma lactate dehydrogenase (LDH) level was 418.7±134.7. No patient had previously received other therapies.

Blood collection

All human blood samples (up to 30 mL) were obtained via informed consent through the Azienda Ospedaliero Universitaria di Modena and Reggio Emilia. Approval of study protocols was obtained by the ethical committee (Prot AOU 0005400/18). Blood was obtained before therapy (hereafter indicated as T0), after the first and the second cycle of therapy (hereafter indicated as T1 and T2 respectively). Peripheral blood mononuclear cells (PBMC) were isolated according to standard procedures and stored in liquid nitrogen until use [40]. The whole experimental procedure is represented in **Supplementary Figure 1**.

Polychromatic flow cytometry

A 30 parameter/28-color flow cytometry panel was optimized to broadly characterizes T cell differentiation and activation along with markers that are target or are involved in immunotherapy response (CD3, CD4, CD8, CD45RA, CD197, CD28, CD27, CD127, CD95, CD98, CD71, CD25, HLA-DR, CD38, CD39, CXCR6, CCR4, KI67, T-bet, granulysin, PD1, BTLA, CD244 and ICOS). Moreover, the panel was optimized to identify the expression of PD1 in T cells isolated from patients treated with anti-PD1 (either nivolumab or pembrolizumab) as anti-IgG4 was used to recognize the anti-PD1 bound to PD1 [27].

Briefly, cryopreserved samples were thawed in R10 medium, *i.e.,* RPMI supplemented with 10% foetal bovine serum (FBS), 100 U/mL penicillin, 100 μg/mL streptavidin, 2 mM L-glutamine, 20 mM HEPES (ThermoFisher, Eugene, OR) and 20 μg/ml DNase I from bovine pancreas (Sigma-Aldrich, St. Louis, MO). After washing with phosphate buffer saline (PBS), cells were stained immediately with the Zombie Aqua Fixable Viability kit (BioLegend, San Diego, CA) for 15 min at

485 room temperature. Then, cells were washed and stained with the combination of monoclonal
486 antibodies (mAbs) purchased from either Becton Dickinson Biosciences (BD, San José, CA),
487 BioLegend, or eBioscience/ThermoFisher (Eugene, OR), as listed in **Supplementary Table 1**, that
488 reports also the fluorochromes bound to the different monoclonal mAbs, that had been previously
489 titrated to define the optimal concentration. Chemokine receptors were stained for 20 min at 37°C,
490 for 20 min at room temperature. Intracellular detection of Ki-67, granulysin and T-bet was
491 performed following fixation of cells with the FoxP3 transcription factor staining buffer set
492 (eBioscience/ThermoFisher) according to manufacturer's instructions and by incubating with
493 specific mAbs for 30 min at 4°C. Samples were acquired on a FACS Symphony A5 flow cytometer
494 (BD Biosciences) equipped with five lasers (UV, 350 nm; violet, 405 nm; blue, 488; yellow/green,
495 561 nm; red, 640 nm) and capable to detect 30 parameters. Flow cytometry data were compensated
496 in FlowJo by using single stained controls (BD Compbeads incubated with fluorochrome-
497 conjugated antibodies) [41]. Gating strategy is shown in **Supplementary Figure 1.**
498 A 18 parameter/16-color flow cytometry panel was then optimized to broadly investigate
499 mucosal invariant associated T (MAIT) cell phenotype, including CD3, CD8, TCR Vα7.2, CD161,
500 CD45RO, CD197, CD28, CD27, CD127, CD95, CD25, HLA-DR, CD38, CXCR4, KI67,
501 granulysin, CD69. Briefly, cryopreserved samples were thawed and stained immediately with
502 PromoFluor-840, viability probe (PromoCell - PromoKine) for 20 min at room temperature. Then,
503 cells were washed and stained with the combination of mAbs purchased from either BD
504 Biosciences, BioLegend, or eBioscience, as listed in **Supplementary Table 2**. mAbs were
505 previously titrated to define the optimal concentration. Chemokine receptors were stained for 20
506 min at 37°C, whereas all the other markers were stained for 20 min at room temperature.
507 Intracellular detection of Ki-67 and granulysin was performed following fixation of cells with the
508 FoxP3/ transcription factor staining buffer set (eBioscience, ThermoFisher) according to
509 manufacturer's instructions and by incubating with specific mAbs for 30 min at 4°C. Samples were
510 acquired on a Cytoflex LX flow cytometer (Beckman Coulter, Hialeah, FL) equipped with six
511 lasers (UV, 355 nm; violet, 405 nm; blue, 488; yellow/green, 561 nm; red, 638 nm; IR, 808nm) and
512 capable to detect 21 parameters. Flow cytometry data were compensated in FlowJo by using single
513 stained controls, as above [41]. Gating strategy is shown in **Supplementary Figure 5**.
514 In parallel, thawed PBMC were rested for 4 hours at 37°C and then *in vitro* stimulated with
515 anti-CD3/CD28 (1μg/ml) (Miltenyi, Bergisch Gladbach, Germany) and suboptimal concentration
516 of IL-12 (2 ng/mL) (Miltenyi) and IL-18 (50 ng/mL) (R&D System, Minneapolis, MN) and a
517 combination of those [25]. A 11 parameter/10-color flow cytometer panel was optimized to identify
518 MAIT cells producing Granzyme (GRZM) A, GRZM B, TNF-α and IFN-γ that were detected after

16 hours of incubation (**Supplementary Table 3**). For the quantification of intracellular cytokines, cells were fixed with BD Cytofix/Cytoperm Fixation/Permeabilization Solution kit (BD Biosciences) according to the manufacturer's instructions. Samples were acquired on an Attune NxT acoustic flow cytometer (ThermoFisher) equipped with four lasers (violet, 405 nm; blue, 488; yellow/green, 561 nm; red, 640 nm) and capable to detect 14 parameters. Flow cytometry data were compensated in FlowJo by using single stained controls as above. Gating strategy is shown in **Supplementary Figure 6.**

High-dimensional flow cytometry data analysis

Flow Cytometry Standard (FCS) 3.0 files were analysed using FlowJo software V 9.6. Aggregates and dead cells were removed from the analyses and identify $CD3^+$ $CD8^+$ T cells were gated. 10,000 CD8+ T cells per sample were exported and biexponentially transformed in FlowJo V10. Further analyses were performed by a custom-made script that makes use of Bioconductor libraries and R statistical packages [4]. Data were analyzed using the Phenograph algorithm coded in the Cytofkit package (version 1.6.5; [42]) in R (version 3.3.3). Parameter K was set at 60. Phenograph clusters were visualized using tSNE. Clusters representing <0.5% were not analysed in subsequent analysis. New FCS files (one for each cluster), originated from Phenograph analyses, were imported and analyzed in FlowJo to determine the frequency of positive cells for each marker and the corresponding median fluorescence intensity (MFI). These values were multiplied to derive the integrated MFI (iMFI, rescaled to values from 0 to 100). gplots R package was used to generate the heat map, showing the iMFI of each marker per cluster [4,43].

Cell Sorting and single cell RNA-sequencing (sc-RNAseq) library preparation

Cryopreserved samples were thawed in R10 supplemented with 20 μg/ml DNase I from bovine pancreas (Sigma-Aldrich). After washing with phosphate buffer saline (PBS), cells were stained with the Red Live Dead Fixable Viability kit (ThermoFisher) for 15 min at room temperature. PBMC were washed with PBS and stained with mAb anti-CD3-PE and -CD8-FITC. Viable $CD3^+$,$CD8^+$ T cells were sorted by using eS3 sorter (Bio-Rad Laboratories, Hercules, CA) equipped with two lasers (blue, 488; yellow/green, 561 nm; all tuned at 100 mW). Cell sorting was performed with 96-99% purity. Sorted CD3+CD8+ T cells were immediately loaded on ddSEQ single-cell isolator (Bio-Rad Laboratories) to isolate single cells and barcode single cells. sc-RNA-seq libraries were prepared by using the Illumina Bio-Rad SureCell WTA 3' Library Prep Kit (Illumina, San Diego, CA, manufactured for Bio-Rad) following manufacturer's instructions. Briefly, after barcoding, RNA was reverse transcribed and cleaned up. Then, second strand cDNA

was synthesized and tagmented. Tagmented DNA was amplified and final indexed libraries were quantified by using the high sensitivity DNA kit (Agilent) on a bioanalyzer (Agilent). Sequenced libraries were loaded on an Illumina MySeq.

sc-RNAseq analyses

Starting from a total of 74,405 cells, 55,200 were deemed suitable for analysis. Downstream analysis was performed in R using Seurat v3.0 [44]. Cells that had less than 10% of mitochondrial genes, read counts of at least 150 genes and less than 1,500 genes were kept for the following analysis. The quality of cells was assessed applying a threshold on the percentage of mitochondrial genes, on number of UMI and gene count. A cluster of 200 cells featuring genes related to the myeloid lineage was excluded from the analysis. Additional 3,010 cells were excluded due to technical artifacts during library preparation. Genes expressed in less than three cells were excluded, then each gene expression measurement was normalized by total expression in the corresponding cell and multiplied by a scaling factor of 10,000 and natural log-transform the result. Previous steps were performed on T0, T1, T2 dataset. Subsequently, all three datasets were integrated yielding an expression matrix of 51,701 cells by 17,745 genes [45].

Principal components were selected using the jackstraw and Elbow methods. The dimensional reduction was performed using Uniform Manifold Approximation and Projection (UMAP) on the previously selected principal components. Unsupervised clustering was performed by finding the nearest neighbors (KNN) and then, to group the cells, a modularity optimization-based algorithm was applied.

The resolution was selected using clustree package [46]. Differentially expressed genes were identified using the FindAllMarkers function, and the top 15 genes for each cluster were visualized in a heatmap. Differential expression analysis was performed between each cluster and all other cells using a Wilcoxon rank-sum test. Genes were selected to be significant as logFC>0.3 and adjusted p value <0.05. Cells from a single cluster were selected and re-clustered to identify the presence of subpopulation. Comparative analyses across conditions inside of each cluster was performed using FindMarkers, genes were considered as significant with logFC > 0.3 and adjusted p value <0.05. Furthermore, a random subset was performed on all 51,701 cells selecting 4,000 cells and then a trajectory analysis was performed using Monocle v2 [47].

cTP-net analysis

The surface protein imputation was performed using a pre-trained deep neural network (cTP-net) trained on PBMC processed using multi-omics approach (CITE-seq and REAP-seq) [21]. cTP-net

predict the following list of surface proteins: CD3, CD4, CD45RA, CD45RO, CD16, CD14, CD11c, CD19, CD8, CD34, CD56, CD57, CD2, CD11a, CD123, CD127-IL7Ra, CD161, CD27, CD278-ICOS, CD28, CD38, CD69, CD79b and HLA-DR. The imputation of surface proteins on our data set was performed using integrated and normalised data.

GSEA analysis

The scRNAseq data were retrieved from the Gene Expression Omnibus (GSE) 148190. The analysis was restricted to K383, K409 and K411 samples containing blood (B), lymph nodes metastasis (LN) or Tumour (T) data. The data set used were GSM4455931, GSM4455932, GSM4455933, GSM4455935, GSM4455937 and GSM4455938. Data from each data set were cleaned selecting the cells expressing less than 10% of mitochondrial genes, read counts of at least 200 genes and less than 3000 genes. Then all data set were integrated and normalized yielding a total of 26,757 (11,614 of B, 12,915 of LN and 2,170 of T). We performed clustering and dimensional reduction using UMAP (see methods) finding 10 clusters at the resolution of 0.3. Signature of each cluster was obtained by using 'FindConservedMarkers' function coded in the Seurat R package. MAIT signature was confirmed by using GeneOverlap [48] **(Supplementary Figure 6)**.

Statistical analysis

Statistical analyses were performed using GraphPad Prism version 6 (GraphPad Software Inc., La Jolla, USA), unless specified otherwise. Significance of differences for the frequency of single Phenograph clusters was determined using two-way ANOVA with Bonferroni post-hoc test. To compare distributions of manually gated subsets significance was determined by paired Wilcoxon t test, unless otherwise specified in the figure legends. Simplified Presentation of Incredibly Complex Evaluation (SPICE) software (version 6, kindly provided by Dr. Mario Roederer, Vaccine Research Center, NIAID, NIH, Bethesda, MD, USA) was used to analyse flow cytometry data on T cell polyfunctionality [49]. Comparison of the curves of response to therapy was performed by Log-Rank (Mantel-Cox) test and p value was considered significant <0.05.

Figure Legends

Figure 1. High-dimensional single cell analysis of CD8+ T cells identifies higher percentage of activated effector memory T cells in responders.

A) Heatmap showing the iMFI of specific markers in discrete Phenograph clusters. Ballons indicate the median frequency of each cluster amongst responders and non-responders. **B)** Individual values of cells present in each cluster. Data represent individual values, mean (centre bar) ± SEM (upper and lower bars). Statistical analysis by two-sided Mann–Whitney nonparametric test; if not indicated, p value is not significant. T0= before therapy, T1=after 1 cycle of therapy, T2=after two cycles of therapy.

Figure 2. MAIT cells are more abundant in responders as revealed by scRNA-seq.

A) UMAP plot. Cells are coloured according to the 8 clusters defined in an unsupervised manner. **B)** Heatmap displaying scaled-expression values of discriminative gene set per cluster related to $CD3^+$,$CD8^+$ T cells that passed quality control. A list of the most representative genes is shown per each cluster (left). N, naive; EMRA, effector memory expressing CD45RA; TM, transitional memory; M, memory; EM, effector memory; MAIT, mucosal associated invariant T cells. **C)** Percentage of activated effector memory (EM) CD8+ T cells at different time points (left) and differential gene expression in this cluster between responders and non-responders at T2 (right). **D)** Percentage of MAIT cells and differential gene expression of this cluster between responders and non-responders at T0, T1 and T2 (right). Data represent individual values, mean (centre bar) ± SEM (upper and lower bars). Statistical analysis by two-sided Mann–Whitney nonparametric test; if not indicated, p value is not significant. Source data are provided as a Source Data file.
T0= before therapy, T1=after 1 cycle of therapy, T2=after two cycles of therapy.

Figure 3. Activated MAIT cells with homing properties are more abundant in responders.

A) UMAP plot of MAIT cells. Not activated MAIT are in salmon and activated ones are in light blue. **B)** Heatmap displaying scaled-expression values of discriminative gene set per each cluster of MAIT cells. A list of representative genes is shown on the left. **C)** Left part: UMAP plot representing two clusters of MAIT cells between R and NR at T0, T1, T2. Right part: Percentage of activated MAIT cells between R and NR at T0, T1, T2. * $p<0.05$; ** $p<0.01$. Statistical analysis by two-sided Mann–Whitney nonparametric test.

Figure 4. MAIT polyfunctionality evaluated after *in vitro* stimulation in PBMC of melanoma patients.

A) Left and centre panels: representative dot plots of MAIT cells, identified as TCR 7.2$^+$ and CD161+ within CD8+ T cells of one R and one NR at T0. Right part: proportion of MAIT cells in R and NR at T0, T1, T2. Statistical analysis by two-sided Mann–Whitney nonparametric test. **B)** Left panel: UMAP representation of PBMCs or tumour-infiltrating lymphocytes from patients with metastatic melanoma. Expression of KLRB1, CD69 and CXCR4 MAIT cells in blood(B), lymph nodes metastasis (LN) and Tumour(T) from the K383, K409 and K411 patients (Gene Expression Omnibus, GSE148190). Right panel: proportion of MAIT in blood (B), lymphnode (LN) and tumour (T). C) Left and central panels: pie charts representing the proportion of MAIT cells producing different combinations of IL-2, IFNγ, and TNF after stimulation. Frequencies were corrected by background subtraction as determined in unstimulated controls; permutation tests, using SPICE software, shows no difference between R and NR. Right panel: frequency of MAIT cells expressing and producing different combinations of IL-2, IFN-γ, and TNF after stimulation. Statistical analysis by two-sided Mann–Whitney nonparametric test; no significant differences were found between R and NR. **D**) Left and central panels: dot plots show the difference between a R and a NR in the percentage of cells that produce IFN-γ and GRZM-B. Right part, percentage of these cells at different time points. Data are given as mean ± SEM. *, $p< 0.05$, Statistical analysis by two-sided Mann–Whitney nonparametric test; no significant differences were found between R and NR.

Figure 5. Level of MAIT cells before therapy can predict initial response to therapy.

Analysis of the cohort patients with metastatic melanoma indicates that patients with MAIT cells >1.7% of CD3$^+$,CD8$^+$ T lymphocytes showed a better response to therapy compared to those with MAIT <1.7% ($p=0.0363$, Log-rank Mantel-Cox test).

Figures

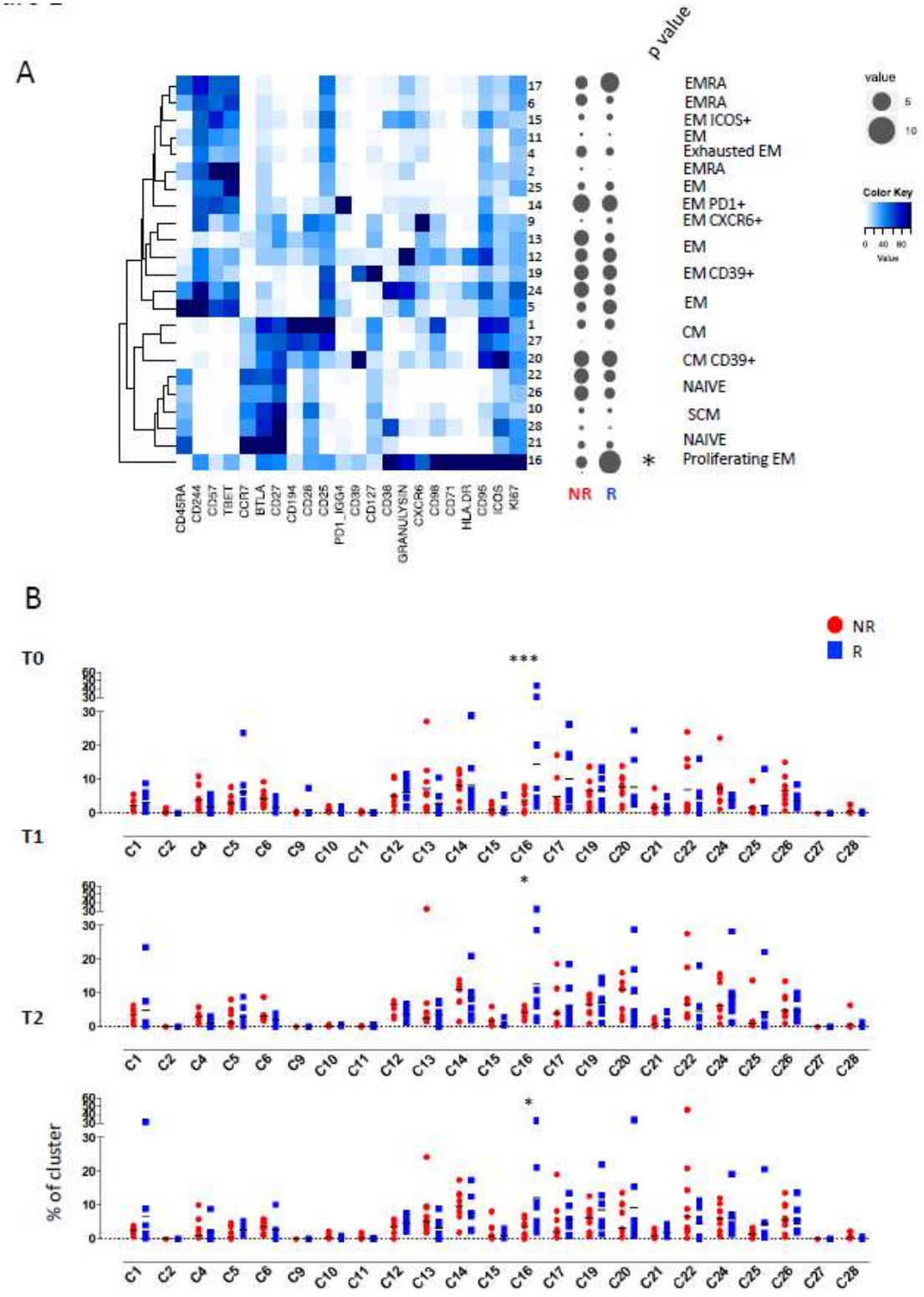

Figure 1

High-dimensional single cell analysis of CD8+ T cells identifies higher percentage of activated effector memory T cells in responders. A) Heatmap showing the iMFI of specific markers in discrete Phenograph clusters. Ballons indicate the median frequency of each cluster amongst responders and non-responders.

B) Individual values of cells present in each cluster. Data represent individual values, mean (centre bar) ± SEM (upper and lower bars). Statistical analysis by two-sided Mann–Whitney nonparametric test; if not indicated, p value is not significant. T0= before therapy, T1=after 1 cycle of therapy, T2=after two cycles of therapy.

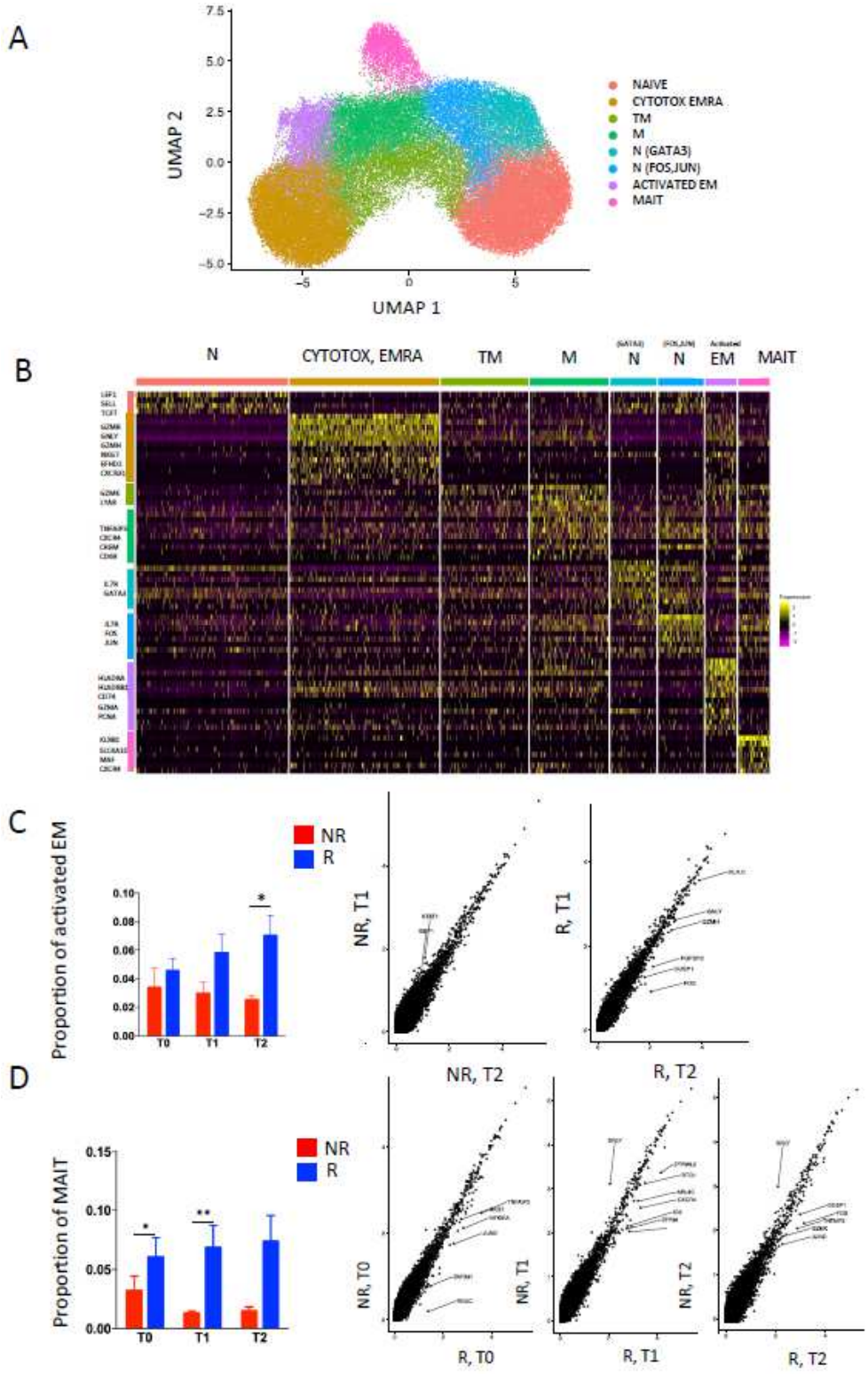

Figure 2

MAIT cells are more abundant in responders as revealed by scRNA-seq. A) UMAP plot. Cells are coloured according to the 8 clusters defined in an unsupervised manner. B) Heatmap displaying scaled-expression values of discriminative gene set per cluster related to CD3+,CD8+ T cells that passed quality control. A list of the most representative genes is shown per each cluster (left). N, naive; EMRA, effector memory expressing CD45RA; TM, transitional memory; M, memory; EM, effector memory; MAIT, mucosal associated invariant T cells. C) Percentage of activated effector memory (EM) CD8+ T cells at different time points (left) and differential gene expression in this cluster between responders and non-responders at T2 (right). D) Percentage of MAIT cells and differential gene expression of this cluster between responders and non-responders at T0, T1 and T2 (right). Data represent individual values, mean (centre bar) ± SEM (upper and lower bars). Statistical analysis by two-sided Mann–Whitney nonparametric test; if not indicated, p value is not significant. Source data are provided as a Source Data file. T0= before therapy, T1=after 1 cycle of therapy, T2=after two cycles of therapy.

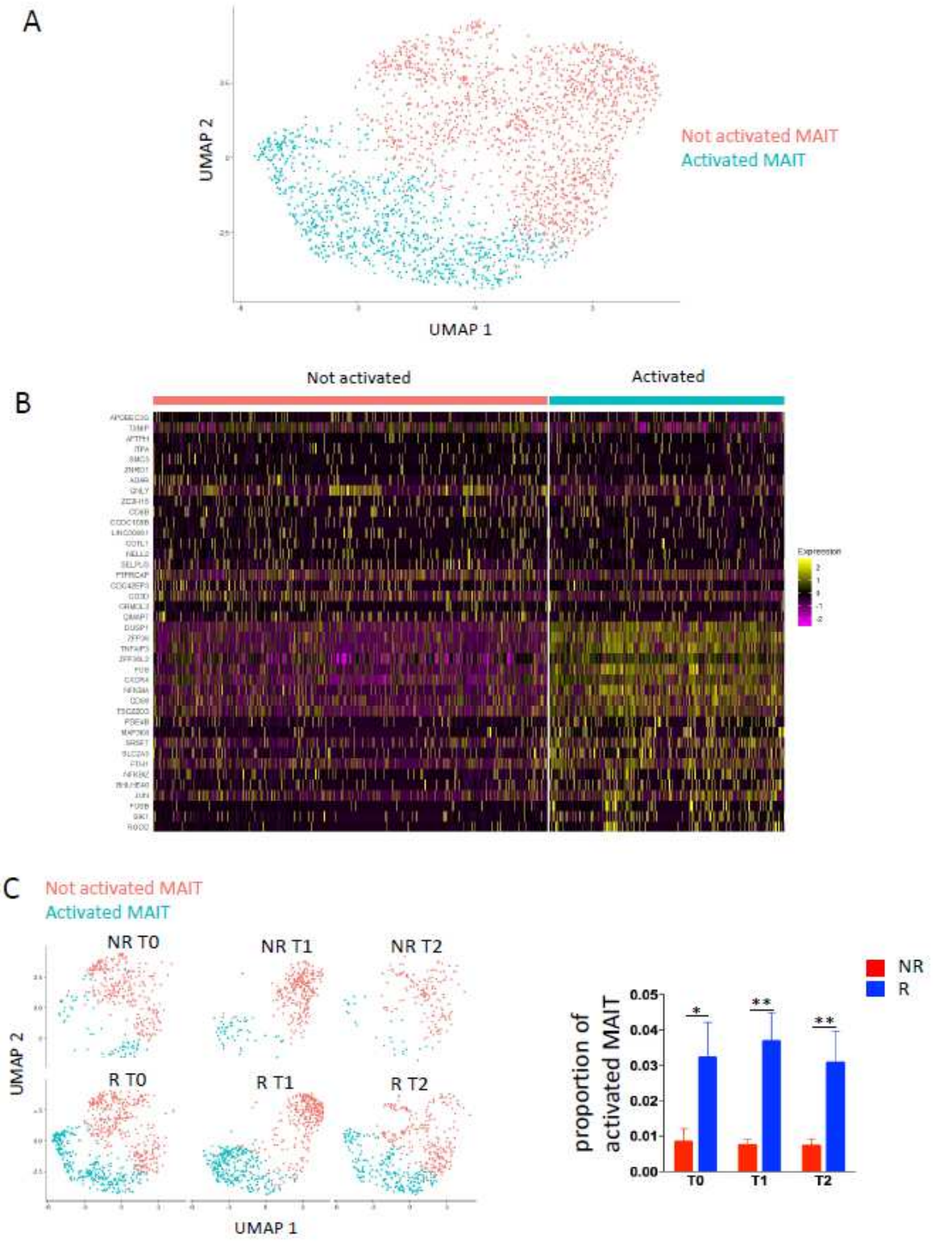

Figure 3

Activated MAIT cells with homing properties are more abundant in responders. A) UMAP plot of MAIT cells. Not activated MAIT are in salmon and activated ones are in light blue. B) Heatmap displaying scaled-expression values of discriminative gene set per each cluster of MAIT cells. A list of representative genes is shown on the left. C) Left part: UMAP plot representing two clusters of MAIT cells between R and

NR at T0, T1, T2. Right part: Percentage of activated MAIT cells between R and NR at T0, T1, T2. * p<0.05; ** p<0.01. Statistical analysis by two-sided Mann–Whitney nonparametric test.

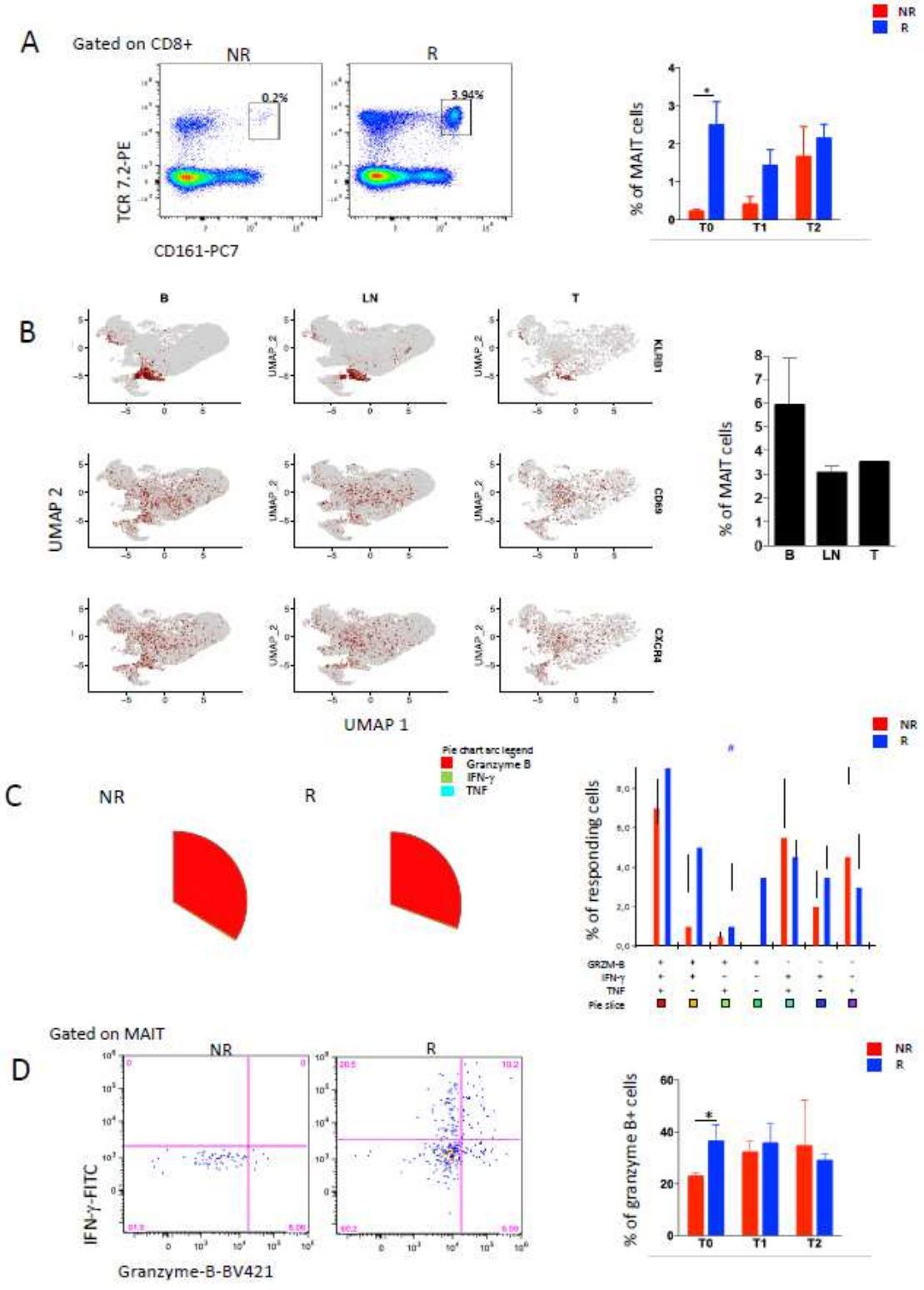

Figure 4

MAIT polyfunctionality evaluated after in vitro stimulation in PBMC of melanoma patients. A) Left and centre panels: representative dot plots of MAIT cells, identified as TCR 7.2+ and CD161+ within CD8+ T cells of one R and one NR at T0. Right part: proportion of MAIT cells in R and NR at T0, T1, T2. Statistical

analysis by two-sided Mann–Whitney nonparametric test. B) Left panel: UMAP representation of PBMCs or tumour-infiltrating lymphocytes from patients with metastatic melanoma. Expression of KLRB1, CD69 and CXCR4 MAIT cells in blood(B), lymph nodes metastasis (LN) and Tumour(T) from the K383, K409 and K411 patients (Gene Expression Omnibus, GSE148190). Right panel: proportion of MAIT in blood (B), lymphnode (LN) and tumour (T). C) Left and central panels: pie charts representing the proportion of MAIT cells producing different combinations of IL-2, IFNγ, and TNF after stimulation. Frequencies were corrected by background subtraction as determined in unstimulated controls; permutation tests, using SPICE software, shows no difference between R and NR. Right panel: frequency of MAIT cells expressing and producing different combinations of IL-2, IFN-γ, and TNF after stimulation. Statistical analysis by two-sided Mann–Whitney nonparametric test; no significant differences were found between R and NR. D) Left and central panels: dot plots show the difference between a R and a NR in the percentage of cells that produce IFN-g and GRZM-B. Right part, percentage of these cells at different time points. Data are given as mean ± SEM. *, p< 0.05, Statistical analysis by two sided Mann–Whitney nonparametric test; no significant differences were found between R and NR.

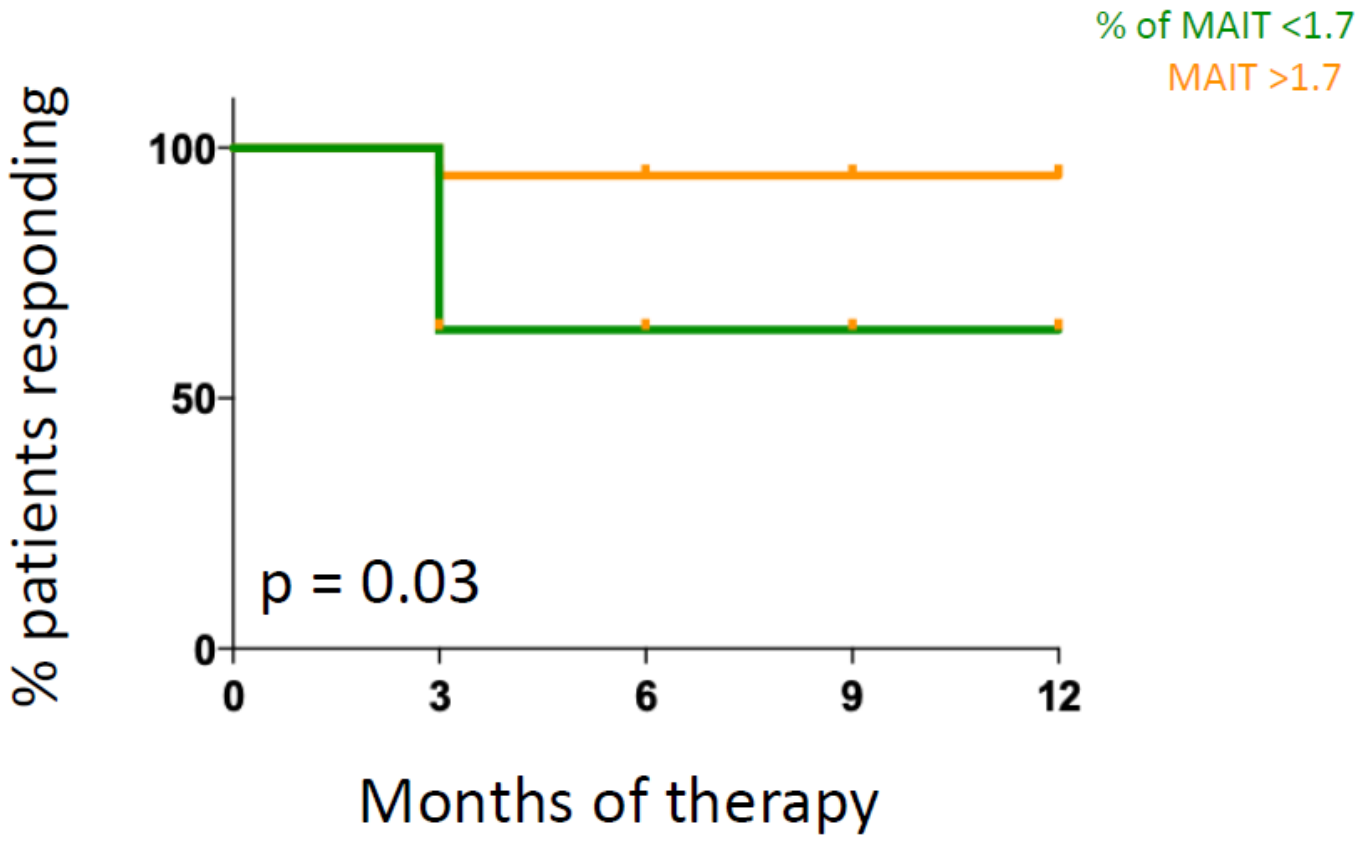

Figure 5

Level of MAIT cells before therapy can predict initial response to therapy. Analysis of the cohort patients with metastatic melanoma indicates that patients with MAIT cells >1.7% of CD3+,CD8+ T lymphocytes

showed a better response to therapy compared to those with MAIT <1.7% (p=0.0363, Log-rank Mantel-Cox test).

Supplementary Files

This is a list of supplementary files associated with this preprint. Click to download.

- SupplementaryTable1.docx
- SupplementaryTable2.docx
- SupplementaryTable3.docx
- SupplementaryFigsmela.pptx
- Supplementaryfilegenesignature.xlsx